Solid Solutions of Plastic/Ferroelectric Crystals: Toward Tailor-Made Functional Materials

Jun Harada,[*,†,‡] Mika Takehisa,[†] Yuto Kawamura,[‡] Hiroyuki Hasegawa,[#] and Tomoyasu Usui[§]

[†]Department of Chemistry, Faculty of Science, and [‡]Graduate School of Chemical Sciences and Engineering, Hokkaido University, Sapporo 060-0810, Japan

[#]Faculty of Education, Shimane University, Matsue, Shimane 690-8504, Japan

[§]Murata Manufacturing Co., Ltd., Kyoto 617-8555, Japan

ABSTRACT: Plastic crystals that show ferroelectricity are highly promising materials for a wide range of applications. Their inherent remarkable malleability and highly symmetric cubic structures in the plastic crystal phase ensure that their ferroelectricity and related properties are retained in their bulk polycrystals. To develop functional materials based on such plastic/ferroelectric crystals, methods to tune their properties for specific applications are required. Here, we report the preparation of solid solutions of plastic/ferroelectric ionic crystals by mixing crystals with a common anion but different cations, or crystals with a common cation but different anions, which allows a continuous modification of the Curie temperature of the ferroelectric system over a range of 100 K. This adjustment of the Curie temperature allows the flexible tuning of the pyroelectric properties of the solid solutions, including a significant enhancement of room-temperature performance. The solid solutions also exhibit morphotropic phase boundaries in the composition–temperature phase diagrams, which shows an abrupt change in crystal structures with a variation of composition. This study showcases a simple and versatile property-tuning method that can be expected to pave the way for a major progress in the development of materials based on plastic/ferroelectric crystals, which will eventually advance to the stage of pursuing tailor-made functional materials with desired properties.

INTRODUCTION

Ferroelectric materials exhibit a spontaneous electric polarization whose direction can be switched by applying an electric field.[1] In addition to the switchable spontaneous polarization, ferroelectric materials possess different related properties, such as pyroelectricity, piezoelectricity, and optical second harmonic generation, which have been employed in applications including non-volatile memory elements, sensors, and actuators. Molecular ferroelectric crystals have recently attracted considerable attention for their potential applications as alternatives or complements to widely used toxic lead-based ferroelectric perovskite oxides.[2]

Among the small-molecule-based ferroelectric crystals, plastic crystals that exhibit ferroelectricity are attracting growing interest due to their unique properties and ease of development.[3,4] Plastic/ferroelectric crystals possess a plastic crystal phase as the high-temperature paraelectric phase and ferroelectric phases as low-temperature phases. The plastic crystal phase is a mesophase between the solid and liquid states, which is often observed in compounds of neutral or ionic molecules with globular molecular structures.[5] In the plastic crystal phase, the globular molecules rotate isotropically and their orientation is completely disordered, albeit that they retain long-range positional order and form crystal lattices similar to those in normal crystals.[6] Plastic crystals undergo one or more solid–solid phase transitions upon cooling and become normal crystals with ordered molecular orientation at low temperatures. In addition to plastic/ferroelectric crystals, plastic crystals have been employed to develop other functional materials such as solid-state ion conductors[7] and barocaloric materials.[8]

Plastic/ferroelectric crystals possess several valuable features not accessible in conventional molecular ferroelectrics, which render the materials highly promising for practical applications. Plastic/ferroelectric crystals show multiaxial ferroelectricity, which allows the polar axis of the crystal to be changed in several different directions in response to an applied electric field. The three-dimensional polarization switching is related to the highly symmetric cubic crystal structures in the plastic crystal phase and is not available for uniaxial molecular ferroelectrics with low crystal symmetry, where only 180°-reversal of polarization is allowed.[4,9] Moreover, monolithic bulk polycrystals can be easily prepared by applying pressure to their powders, because the plastic crystals are highly malleable and easily deformed without fracturing under compressive stress. The multiaxial ferroelectricity and high malleability of plastic/ferroelectric crystals allowed, for the first time, ferroelectric performance to be achieved in bulk small-molecule polycrystals, *e.g.*, compacted pellets of powders.[3] Thus, both in terms of performance in polycrystalline forms and the ready availability of monolithic bulk polycrystals, plastic/ferroelectric crystals share the strengths of ferroelectric inorganic perovskite oxides such as barium titanate and lead zirconate titanate, which are widely used as ferroelectric ceramics in industry owing to these advantages.

Since the first report, a multitude of plastic/ferroelectric crystals with various characteristics have been developed based on ionic molecules by combining cations and anions with globular molecular structures.[10] To further develop these emerging functional materials, a means of tuning and optimizing the properties of existing crystals and preparing tailor-made materials for

specific applications is required. Here, we demonstrate a method for tuning the property of plastic/ferroelectric ionic molecular crystals via a rational solid-solution formation technique.

The formation of solid solutions, also called mixed crystals or alloys, is a widely applied property-tuning strategy and the key to the successful industrial applications of ferroelectric inorganic perovskite oxides.[11] For example, substitution of the constituent metal ions of $BaTiO_3$, *i.e.*, Ba^{2+} and Ti^{4+}, with ions such as Sn^{4+}, Pb^{2+}, Sr^{2+}, Ca^{2+}, or Mg^{2+}, allows tuning the dielectric properties to obtain desired characteristics through shifting the temperature of or depressing the sharpness of the dielectric constant peak of $BaTiO_3$. Moreover, solid solutions of ferroelectric $PbTiO_3$ with antiferroelectric $PbZrO_3$ (PZT) or relaxor $Pb(Mg_{1/3}Nb_{2/3})O_3$ (PMN–PT) show a morphotropic phase boundary (MPB) in their composition–temperature phase diagrams.[11,12] A morphotropic transition is defined as an abrupt change in the crystal structure of the solid solutions with variation in composition, and electromechanical and dielectric responses of these ferroelectric solid solutions exhibit a significant enhancement in the vicinity of the MPB. Also, an organic–inorganic hybrid cadmium-halide one-dimensional perovskite has been reported to show a significant enhancement of piezoelectricity near the MPB, which is induced through solid-solution formation by mixing organic cations,[13] while changes in the crystal structure and ferroelectric transition temperature with compositional variation has recently been achieved in lead-halide two-dimensional perovskite ferroelectrics through enantiomeric organic cation mixing (*i.e.*, racemization).[14]

In this study, we report on the utility of a simple precipitation-based method to prepare solid solutions of the plastic/ferroelectric ionic crystal 1-azabicyclo[2.2.1]heptanium perrhenate ([AH][ReO_4]). [AH][ReO_4] is a highly promising plastic/ferroelectric crystal that shows ferroelectric switching under low electric fields and exhibits extremely high pyroelectric performance in polycrystals.[15] Rapid precipitation from a mixed solution of [AH][ReO_4] and plastic/ferroelectric ionic molecular crystals with a different cation or anion, *i.e.*, quinuclidinium perrhenate ([QH][ReO_4])[3] or 1-azabicyclo[2.2.1]heptanium periodate ([AH][IO_4]),[15] resulted in all-proportional solid solutions, which cannot be obtained via other commonly employed crystal-growth methods. The mixed-anion or mixed-cation solid solutions allowed continuous tuning of the ferroelectric transition temperature over a range of 100 K and significantly enhanced the materials' utility as pyroelectrics. We also found that MPBs and a novel phase emerge in the phase diagrams of the solid solutions. This report thus represents the first example of such property tuning in plastic/ferroelectric crystals. This versatile tuning method is potentially applicable to other related compounds and can be expected to greatly extend the utility of this class of functional materials.

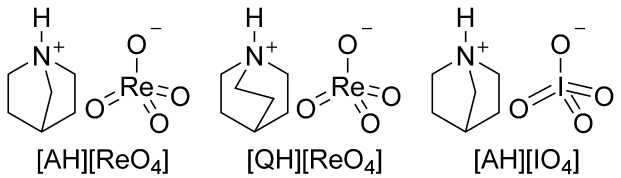

EXPERIMENTAL SECTION

Materials. [AH][ReO_4], [QH][ReO_4], and [AH][IO_4] were prepared as white powders according to literature procedures.[3,15] Solid solutions of the aforementioned salts were obtained by preparing nearly saturated ethanol solutions of mixtures of the salts in the desired molar ratio, to which five times the volume of hexane was rapidly added under stirring at room temperature. The thus obtained white precipitate was filtered off and subsequently dried under reduced pressure to yield the solid solution, with a typical yield of ~90%. The composition of the solid solutions of [AH][ReO_4] and [QH][ReO_4] (x in [$A_xQ_{1-x}H$][ReO_4]) was determined based on an LC-MS analysis (Waters Acquity UPLC/ZQ2000) by estimating the molar ratio of [AH] and [QH] cations in the sample solutions. The composition of the solid solutions of [AH][ReO_4] and [AH][IO_4] (y in [AH][$Re_yI_{1-y}O_4$]) were determined based on an ICP-MS analysis (Agilent 8800 ICP-QQQ) by estimating the molar ratio between rhenium and iodine atoms in the sample solutions.

Bulk polycrystalline plates of the materials for electrical measurements were prepared by application of uniaxial pressure to the powder in the high-temperature phase, typically at ~100 °C. A photograph of microcrystals and a bulk polycrystalline plate of the solid solution of [$A_{0.5}Q_{0.5}H$][ReO_4] is shown in Figure S1. Scanning electron microscopy (SEM) images of bulk polycrystalline plates of several solid solutions are shown in Figure S2.

Caution! Powders of [AH][IO_4] and its solid solutions are potentially explosive because they contain periodate ions. Although the powders did not explode under normal handling, including heating to 150 °C and pressing at ~100 °C, they did explode when heated with a flame.

RESULTS AND DISCUSSION

Preparation of Solid Solutions [$A_xQ_{1-x}H$][ReO_4] and [AH][$Re_yI_{1-y}O_4$]. Solid solutions of molecular crystals have been studied extensively. It is widely accepted that the formation of solid solutions is limited to those between molecules with similar molecular and crystal structures.[16] Although significant consideration has been given to whether certain combinations of molecules can form stable solid solutions, much less attention has been paid to experimental procedures for preparing solid solutions.[17] Even though crystallization from solution, via *e.g.*, evaporating the solvent or cooling the solution, is the most common and efficient method for preparing solid substances, this process itself can be a major obstacle to the formation of solid solutions with the desired composition. When the constituent compounds exhibit different solubility from each other, the composition of the resulting solid solution often differs from that of the initial solution. In an unfavorable scenario, even if a thermodynamically stable solid solution could exist, crystals with lower solubility grow first, followed by crystals with higher solubility, resulting in a solid mixture with multiple phases rather than a homogeneous single-phase solid solution. To expand the utility of plastic/ferroelectric crystals and other functional molecular crystals, it is essential to develop a convenient high-yielding method that produces homogeneous single-phase solid solutions with a wide compositional range. In this study, we have successfully prepared all-proportional solid solutions of ionic molecular crystals, which has so far not been accomplished using conventional solution-evaporation methods.

We have prepared solid solutions of high-performance plastic/ferroelectric crystals of [AH][ReO_4] by mixing it with crystals that contain the same anion but a different cation ([QH][ReO_4]), or the same cation but a different anion ([AH][IO_4]). Each of the three crystals exhibits three solid

phases: a high-temperature plastic crystal phase (HTP) with CsCl-type cubic structures, and two ferroelectric intermediate- (ITP) and low-temperature phases (LTP), in which the crystals exhibit ferroelectricity due to reorientation of the polar cations.[3,15] We tested several procedures for preparing solid solutions of [AH][ReO_4] and [QH][ReO_4] in a 1:1 molar ratio, and established a standard protocol, *i.e.*, a rapid-precipitation technique that is also applicable to solid solutions with other compositions.

Several solid solutions of ionic plastic crystals have been obtained from solvent evaporation.[18] However, slow evaporation from ethanol or water solutions of [AH][ReO_4] and [QH][ReO_4] mixtures yielded solid mixtures with two different phases after the complete removal of the solvent. The PXRD patterns of the obtained solids were interpreted as superpositions of the patterns of the rhombohedral ITP of [AH][ReO_4] and the orthorhombic LTP of [QH][ReO_4], which are the stable phases of the respective crystals at room temperature (Figure S3). These results indicate that [AH][ReO_4] and [QH][ReO_4] crystals formed separately through slow evaporation, although each phase may contain the other component to some extent as a solid solution (Scheme 1).

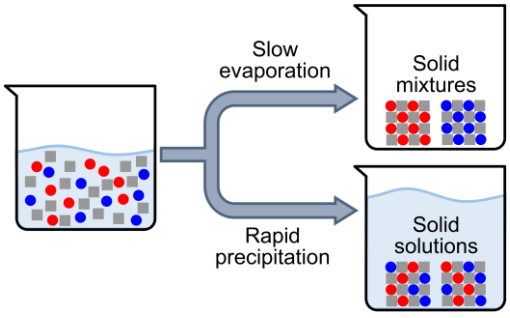

Scheme 1 Difference between slow evaporation of solvent and rapid precipitation from solution of mixtures.

While solid-solution formation by heating polycrystalline disks of binary mixtures of ionic plastic crystals has been reported,[19] the present system remained intact during solid-state heating and did not form solid solutions (Figure S3). Moreover, solid solutions of organic ionic plastic crystals with low melting points have been prepared by solidification of a molten mixture; for example, a dramatic increase in ionic conductivity has been achieved by doping a small amount of lithium ions into the matrix of plastic crystals.[20] However, this method cannot be applied to the present system because the [AH][ReO_4] and [QH][ReO_4] crystals decompose before melting.

In contrast, a solid solution was obtained via rapid precipitation from a solution of [AH][ReO_4] and [QH][ReO_4] in ethanol, a good solvent, by adding five times the volume of hexane, a poor solvent (Scheme 1). The PXRD pattern indicates that the obtained microcrystalline powder represents a single phase with a crystal structure isomorphous to the rhombohedral ITP of [AH][ReO_4] and [QH][ReO_4] (Figure S3). The DSC traces shown in Figure S4 exhibit two sharp peaks corresponding to the two solid–solid phase transitions (HTP/ITP and ITP/LTP), which was also observed for both [AH][ReO_4] and [QH][ReO_4] crystals.

Single-phase solid solutions were also obtained from rotary evaporation, albeit that their quality was lower than those obtained from rapid precipitation. PXRD measurements showed that the rotary evaporation of an ethanol solution provided a single-phase solid solution, while that of a water solution yielded a small amount of the orthorhombic [QH][ReO_4]-type phase in addition to the solid solution (Figure S3). Although the PXRD patterns of the solid solutions obtained from these different methods were similar, the DSC measurements revealed notable differences in their quality (Figure S4). The solid solution obtained from rapid precipitation exhibited sharper peaks compared to those obtained from rotary evaporation. The peak broadening observed for the evaporated solids is probably due to the inhomogeneous distribution of compositions in the samples, *i.e.*, solid solutions with slightly different compositions were formed, each of which undergoes phase transitions at different temperatures, resulting in a broad peak for the overall sample.

Since the solid solutions are forced to crystallize fast during the rapid precipitation, the different solubility of the constituent compounds is not likely to result in selective crystallization. Thus, the obtained solid solutions possess a uniform composition that is similar to the composition of the raw solution, and they thus present sharp peaks in their DSC traces. This also explains the broader peaks for the solid solution obtained from rotary evaporation of the aqueous solution, as the crystallization was slower than that of the ethanol solution.

This rapid precipitation technique provided all-proportional solid solutions for both the [AH][ReO_4]/[QH][ReO_4] and [AH][ReO_4]/[AH][IO_4] systems (Figures S5 and S6); their analyzed compositions were within 2% and 1% of those in the raw solutions, respectively (Tables S1 and S2). All the solid solutions exhibited two solid–solid phase transitions, which gave rise to distinct peaks in the DSC traces (Figure S7). Given that the compositions of the solid solutions obtained in the present method were almost identical to those in the raw material solutions, the solid solutions are hereafter denoted using the composition of the raw solution, *i.e.*, [$A_xQ_{1-x}H$][ReO_4] and [AH][$Re_yI_{1-y}O_4$], where x ($0 \le x \le 1$) and y ($0 \le y \le 1$) represent the molar fraction of [AH][ReO_4]. These results indicate that nonselective crystallization from solutions of the raw material mixtures is the key to preparing solid solutions with homogeneous compositions, and that the rapid-precipitation technique is a simple and efficient method for this purpose.

Continuous Tuning of the Curie Temperature of Solid Solutions. We further found that the Curie temperature (T_C), which is the transition temperature between the ferroelectric and paraelectric phases, of the plastic/ferroelectric crystal [AH][ReO_4] can be changed markedly via the formation of solid solutions. The T_C value of ferroelectric crystals defines their operating temperature window; the crystals exhibit ferroelectricity and related properties only below the T_C. Additionally, the values of several physical properties, such as the dielectric constant and pyroelectricity, reach a maximum as the ferroelectric crystal approaches T_C. Since these values often vary as a function of T_C–T, the properties at the temperature of interest, *e.g.*, room temperature, can be significantly modulated by tuning the T_C. Furthermore, an appropriate T_C is essential for the application of ferroelectric crystals in solid-state cooling using the electrocaloric effect.[21] Therefore, T_C is an important index for functional ferroelectric crystals, and its modification is the primary approach to tailor their characteristics to specific applications.[11]

Solid-solution formation via the rapid-precipitation technique enabled us to continuously vary the T_C over a range of 100 K. The DSC traces of [$A_xQ_{1-x}H$][ReO_4] and [AH][$Re_yI_{1-y}O_4$] shown in Figure 1 for selected compositions and temperature ranges illustrate the changes in T_C (for the

complete data set, see Figure S7). The T_C value of the solid solutions, which was defined as the transition temperature between the ITP and HTP, exhibits a linear dependence on x and y (Figure 1c). As the [AH] concentration x in $[A_xQ_{1-x}H][ReO_4]$ is decreased by substitution with [QH], the T_C increases from 323 K in $x = 1$ ($[AH][ReO_4]$) to 367 K in $x = 0$ ($[QH][ReO_4]$). On the other hand, a decrease in the $[ReO_4]$ concentration y by substitution with $[IO_4]$ lowers the T_C in $[AH][Re_yI_{1-y}O_4]$ to 259 K in $y = 0$ ($[AH][IO_4]$). These results indicate that the T_C of the materials can be easily set to any value between 259 K and 367 K due to the linear dependence of T_C on their compositions, which are virtually identical to those in the raw solutions. This advantage has been utilized in the precise tuning of pyroelectricity described in a later section (*cf. Pyroelectric Properties of Solid Solutions*).

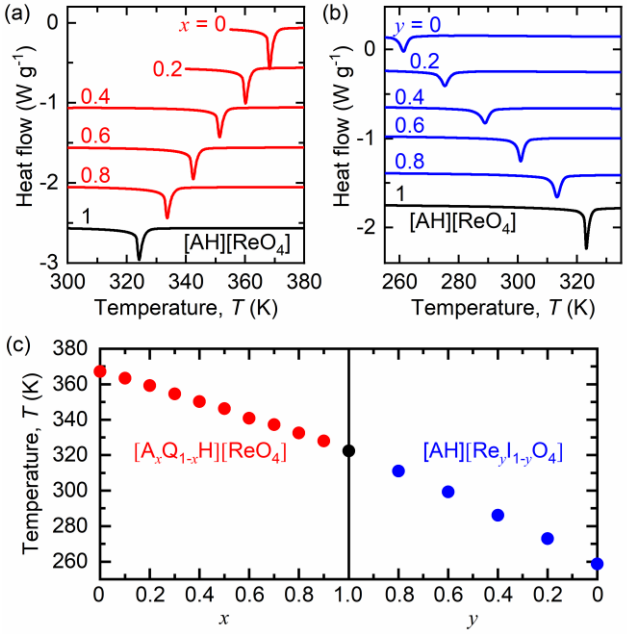

Figure 1. DSC traces of (a) $[A_xQ_{1-x}H][ReO_4]$, (b) $[AH][Re_yI_{1-y}O_4]$, and (c) T_c of $[A_xQ_{1-x}H][ReO_4]$ as well as $[AH][Re_yI_{1-y}O_4]$ as a function of the composition.

PXRD measurements showed that all $[A_xQ_{1-x}H][ReO_4]$ and $[AH][Re_yI_{1-y}O_4]$ solid solutions, as well as the end members ($[AH][ReO_4]$, $[QH][ReO_4]$, and $[AH][IO_4]$) have isomorphous structures in both the paraelectric HTP and the ferroelectric ITP, *i.e.*, the phases immediately above and below the T_C (Figures 2, S5, and S6). Each observed HTP pattern was fitted to the cubic crystal lattice using the Le Bail method, which indicates that the solid solutions are in the plastic crystal phase. The obtained lattice parameter a showed a nearly linear dependence on the composition, obeying Vegard's law (Figure S8).[22] The PXRD patterns in the ITP were also successfully fitted by the trigonal crystal system with the rhombohedral lattice, and the obtained lattice parameters a and α of $[A_xQ_{1-x}H][ReO_4]$ also show almost linear relationships with the composition (Figure S9).

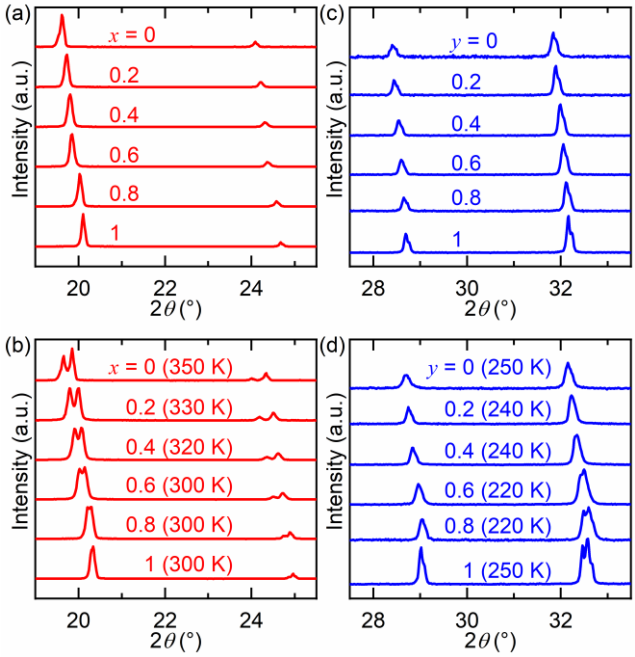

Figure 2. Powder X-ray diffraction patterns of (a) $[A_xQ_{1-x}H][ReO_4]$ in the cubic HTP at 380 K and (b) in the rhombohedral ITP at the indicated temperatures. (c) $[AH][Re_yI_{1-y}O_4]$ in the cubic HTP at 330 K and (d) in the rhombohedral ITP at the indicated temperatures.

Although the crystal lattices of $[AH][Re_yI_{1-y}O_4]$ in the ITP remain nearly cubic, they can be refined as the trigonal crystal system with only slightly distorted pseudo-cubic rhombohedral lattices ($\alpha \approx 90°$) (Table S3). We therefore concluded that all the solid solutions $[A_xQ_{1-x}H][ReO_4]$ and $[AH][Re_yI_{1-y}O_4]$ undergo transitions between the ferroelectric rhombohedral ITP and the paraelectric cubic HTP, whereby the T_C values and lattice geometry continuously vary with the composition. It should also be noted here that the occurrence of the same type of phase transition at different compositions is important for the use of solid solutions as pyroelectric materials, because the high pyroelectricity of $[AH][ReO_4]$ crystals is largely due to the second-order nature of the ITP/HTP phase transition.

Ferroelectric Properties of Solid Solutions. The principal characteristics of $[AH][ReO_4]$ as ferroelectric crystals are preserved in the solid solutions, as shown by the comparable features in the temperature dependence of the dielectric constant and polarization–electric field diagrams. Figure 3 shows the dielectric constant ε' of $[A_xQ_{1-x}H][ReO_4]$ measured using polycrystalline plates as a function of temperature. At the HTP/ITP transition, each solid solution exhibits a sharp peak characteristic of proper ferroelectric–paraelectric phase transitions, and these peaks occur at different temperatures. The ITP/LTP transition at lower temperatures is also found as dielectric anomalies of a step-like change in the ε' values, which is attributable to the onset of orientational polarization due to reorientation of the polar cations, *i.e.*, [AH] and [QH].[3,15] The temperature dependence of ε' of $[AH][Re_yI_{1-y}O_4]$ also exhibited similar features (Figure S10): a sharp peak at the HTP/ITP transitions and small anomalies at the ITP/LTP transitions. These features indicate that the solid-solution formation of $[AH][ReO_4]$ does not significantly change its dielectric behavior associated with phase transitions despite the marked changes in the transition temperatures.

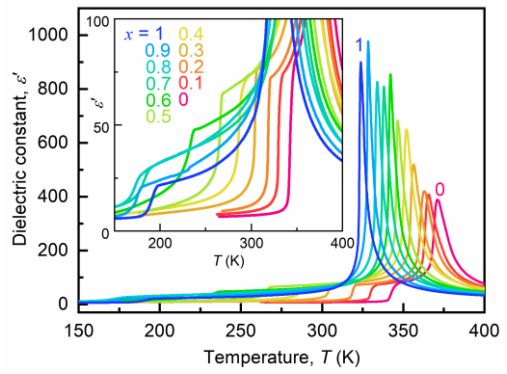

Figure 3. Dielectric constant ε' of polycrystalline plates of $[A_xQ_{1-x}H][ReO_4]$ measured as a function of temperature at a frequency of 10 kHz.

The ferroelectric performance of the $[AH][ReO_4]$ crystals at room temperature was also maintained in the solid solutions $[A_xQ_{1-x}H][ReO_4]$. Whereas both the ITP and LTP of $[AH][ReO_4]$ crystals are ferroelectric phases, the advantageous features as ferroelectric materials, *e.g.*, low-electric-field polarization switching and large pyroelectricity, are limited to the ITP; thus, the existence of the ITP at room temperature makes the $[AH][ReO_4]$ crystals highly promising.[15] Therefore, we focused on the ferroelectric properties of the solid solutions in the ITP; those in the LTP are briefly discussed in a later section (*cf. Characterization of LTPs and Morphotropic Phase Boundaries of Solid Solutions*).

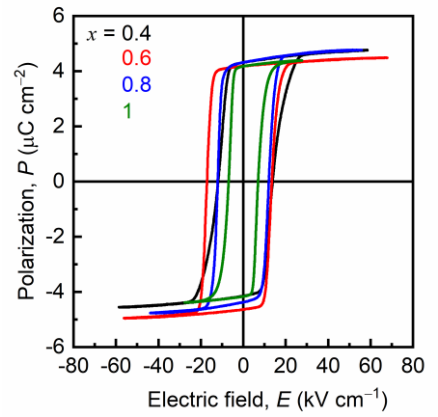

Figure 4. Polarization–electric field (P–E) diagrams of polycrystalline plates of $[A_xQ_{1-x}H][ReO_4]$ in ITP (at 300 K) measured under a triangular electric field (10 Hz).

Figure 4 shows the hysteresis loops in the P–E diagrams of $[A_xQ_{1-x}H][ReO_4]$ (x = 0.4, 0.6, 0.8, and 1) in the ITP measured at 300 K. While the coercive electric fields (E_c) estimated from the intercepts (P = 0) in the loops show some composition-dependent variation (7–15 kV cm^{-1}), the spontaneous polarization (P_s) estimated by the intercepts (E = 0) is almost identical for all solid solutions (4.2–4.4 μC cm^{-2}). Crystals of $[A_xQ_{1-x}H][ReO_4]$ (x = 0, 0.2), which are in the LTP rather than the ITP at 300 K, also showed similar E_c and P_s values in the ITP at elevated temperatures (Figure S11). The P–E hysteresis loops of the $[AH][Re_yI_{1-y}O_4]$ solid solutions in the ITP presented in Figure S12 also exhibit almost constant values for P_s (3.9–4.2 μC cm^{-2}), except in the case of $[AH][IO_4]$ (3.5 μC cm^{-2}), which was measured at a temperature (250 K) close to its T_C (259 K). The $[AH][Re_yI_{1-y}O_4]$ systems still exhibited relatively small E_c values (14–30 kV cm^{-1}) in the ITP despite being measured at low temperatures.

The overall similarity in the ferroelectric properties found in the solid solutions is consistent with their isomorphous crystal structures in the ITP. In particular, the small E_c values of all the solid solutions are highly advantageous for their use as bulk polycrystals, as they allow plates with substantial thickness to be easily subjected to ferroelectric switching and electrical poling. The present strategy for the formation of solid solutions enables a widening of the temperature window of the ITP (182–332 K for $[A_{0.8}Q_{0.2}H][ReO_4]$) for a single-composition crystal, while covering a wide range of temperatures (182–367 K) via an adjustment of the composition (Figure S13).

Pyroelectric Properties of Solid Solutions. We found that the solid solutions based on $[AH][ReO_4]$ exhibit flexibly tunable pyroelectric behavior, which includes a significant enhancement of the pyroelectric performance at room temperature. Pyroelectricity is the temperature dependence of the spontaneous polarization of anisotropic solids, and has found a wide range of applications, such as human-body detection and thermal-energy harvesting.[23] Ferroelectric crystals are a sub-class of pyroelectric crystals, and all ferroelectric crystals show pyroelectricity. The P_s value of ferroelectrics decreases upon heating and, accordingly, the pyroelectric coefficient p (eq 1) becomes negative.

$$p = \frac{dP_s}{dT} \quad (1)$$

Ferroelectrics that exhibit a second-order ferroelectric–paraelectric phase transition are particularly useful for pyroelectric applications. This is because the P_s value of such ferroelectrics gradually decreases upon heating, which results in large $|p|$ values that gradually increase over a wide temperature range as the temperature approaches T_C. Ferroelectrics with a T_C that is not significantly higher than room temperature are especially useful, as they exhibit large $|p|$ values at room temperature. In such ferroelectrics, tuning the T_C can significantly affect the pyroelectric performance of the materials at room temperature.

In addition to large $|p|$ values, a low dielectric constant is advantageous in terms of materials applications. This is because a large voltage response is expected for a given thermal input, since pyroelectric materials usually act as dielectrics in devices. The voltage-related pyroelectric performance of materials can be evaluated using the voltage responsivity (F_v) and the electrothermal coupling factor (k^2), which are defined by eqs 2 and 3, respectively:

$$F_v = \frac{p}{\rho c_p \varepsilon_0 \varepsilon'_{33}} \quad (2)$$

$$k^2 = \frac{p^2 T_{hot}}{\rho c_p \varepsilon_0 \varepsilon'_{33}} \quad (3)$$

where ρ is the density, c_p the specific heat capacity, ε_0 the vacuum permittivity, ε'_{33} the relative dielectric constant measured parallel to the polarization of the poled sample, and T_{hot} the maximum working temperature.[23d] The indices F_v and k^2 are often used for selecting materials for infrared sensors and thermal-energy harvesters, respectively.

Molecular ferroelectric crystals of triglycine sulfate (TGS) are particularly useful as device elements in high-performance infrared sensors due to their high $|p|$ and $|F_v|$ values at room temperature ($|p|$ = 280 μC m^{-2} K^{-1} and $|F_v|$ = 0.36 m^2 C^{-1}).[23b] The

high performance of TGS has been attributed to the synergistic effect of its second-order ferroelectric–paraelectric transition, near-room-temperature T_C (322 K), and small dielectric constant ($\varepsilon'_{33} = 38$), which endow it with one of the highest hitherto reported $|F_v|$ values. The [AH][ReO_4] crystals also undergo a second-order phase transition near room temperature (T_C = 323 K) and exhibit a small dielectric constant ($\varepsilon'_{33} \approx 20$).[15] These features make [AH][ReO_4] crystals high-performance pyroelectrics ($|p|$ = 190 μC m^{-2} K^{-1} and $|F_v|$ = 0.58 m^2 C^{-1} at 298 K) comparable to TGS single crystals, and their performance is available even in bulk polycrystalline forms.[15,24]

The pyroelectric performance of the [AH][ReO_4] crystals can be flexibly tuned by adjusting the T_C to the desired value. Details of the pyroelectric measurements and analysis are described in the Supporting Information (Figures S14–S19 and Tables S4–S6). The formation of the mixed-anion solid solutions [AH][$Re_yI_{1-y}O_4$] decreases the T_C of the system (Figure 1). The resulting proximity of T_C to room temperature enhances the pyroelectricity of the solid solutions. For example, polycrystalline plates of the solid solution [AH][$Re_{0.8}I_{0.2}O_4$] (T_C = 311 K) exhibited a significantly increased $|p|$ value of 290 μC m^{-2} K^{-1} at 298 K (Table S5), and the corresponding $|F_v|$ value was enhanced to 0.80 m^2 C^{-1} at 298 K (Figure 5). This $|F_v|$ value is the highest among hitherto reported polycrystalline materials and is by more than one order of magnitude higher than that of the widely used polycrystalline pyroelectrics of PZT ceramics ($|F_v|$ = 0.059 m^2 C^{-1}).[23b] The k^2 (T_{hot} = 300 K) value of the polycrystals also increased from 3.3% for [AH][ReO_4] to 7.1% for [AH][$Re_{0.8}I_{0.2}O_4$], placing it among the largest values reported so far and much higher than that of PZT ceramics (0.68%).[23d] These results indicate that the obtained solid solutions represent high-performance pyroelectrics for use at room temperature.

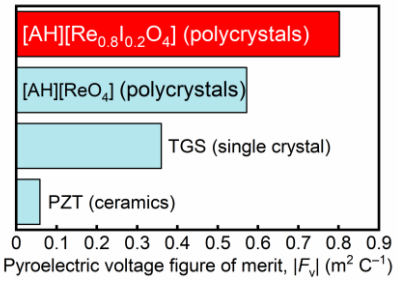

Figure 5. Comparison of pyroelectric voltage responsivity $|F_v|$ at 298 K.

On the other hand, solid-solution formation by substituting the cation [AH] with [QH] increases the T_C values, *e.g.*, T_C = 341 K for [$A_{0.6}Q_{0.4}H$][ReO_4]. Although the solid solution [$A_{0.6}Q_{0.4}H$][ReO_4] shows a smaller $|p|$ value and correspondingly smaller values of $|F_v|$ and k^2 at 298 K ($|p|$ = 100 μC m^{-2} K^{-1}, $|F_v|$ = 0.27 m^2 C^{-1}, and k^2 = 0.80% at 298 K) (Table S6), its pyroelectricity is available at higher temperatures compared to [AH][ReO_4] and [AH][$Re_{0.8}I_{0.2}O_4$], as the pyroelectricity of the materials becomes zero above their T_C. Furthermore, as the T_C of the [$A_{0.6}Q_{0.4}H$][ReO_4] crystals is significantly higher than room temperature, its $|p|$, $|F_v|$, and k^2 values show only a small temperature dependence near room temperature (Figures 6 and S20). It is therefore expected that the [$A_{0.6}Q_{0.4}H$][ReO_4] crystals will display a more constant and stable thermal response under ambient conditions, which may enhance their usability.

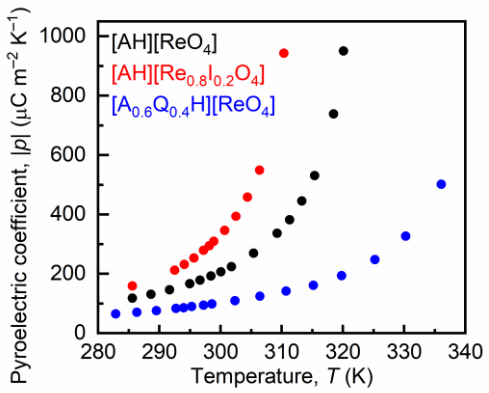

Figure 6. Temperature dependence of the pyroelectric coefficients of polycrystalline plates of [AH][ReO_4], [AH][$Re_{0.8}I_{0.2}O_4$], and [$A_{0.6}Q_{0.4}H$][ReO_4].

The aforementioned results indicate that T_C tuning via solid-solution formation is a simple yet highly effective method that enables the tailored fabrication of high-performance plastic/ferroelectric crystals that exhibit ferroelectricity and pyroelectricity as bulk polycrystals. The pyroelectricity of a single substance is limited below its T_C, and high performance can only be obtained within a specific temperature range. However, solid-solution formation can extend the utility of the substance to various temperature ranges. Notably, in the case of [AH][ReO_4] crystals, the second-order nature of the ferroelectric–paraelectric phase transition does not change upon forming the solid solutions, as indicated by the gradual change in the $|p|$ values with changing temperature. These features allow for the preparation of tailor-made materials with a flexible temperature range for high performance. Such materials are advantageous for a variety of applications, including energy harvesting based on temperature fluctuation at various environmental temperatures.

Characterization of LTPs and Morphotropic Phase Boundaries of Solid Solutions. The LTPs of the mixed-cation solid solutions [$A_xQ_{1-x}H$][ReO_4] were characterized, and MPBs were observed in the phase diagrams. Single-crystal X-ray diffraction studies revealed that [AH][ReO_4] and [QH][ReO_4] share a CsCl-type cubic structure (space group: $Pm\bar{3}m$) in the plastic crystal phase (HTP) and a pseudo-cubic rhombohedral structure (space group: $R3m$) in the ferroelectric ITP.[3,15] This isostructural relationship is consistent with the common crystal structures in the HTP and ITP of the solid solutions [$A_xQ_{1-x}H$][ReO_4] (Figure 2). For the LTP, the structure of [QH][ReO_4] was determined using single-crystal X-ray diffraction analysis (orthorhombic crystal system; space group: $Pmn2_1$),[3] albeit that the structure of [AH][ReO_4] could not be resolved due to inevitable twinning caused by the ITP/LTP transition.[15]

The LTPs of [$A_xQ_{1-x}H$][ReO_4] exhibit three ferroelectric phases with different structures upon varying x. The P–E diagrams of all [$A_xQ_{1-x}H$][ReO_4] samples in the LTPs displayed well-defined hysteresis loops, confirming their ferroelectricity (Figure S21). The P_s values of [$A_xQ_{1-x}H$][ReO_4] in the LTPs (4.3–5.0 μC cm^{-2}) are slightly larger than those in the ITPs (Figures 4 and S11), and the observed E_c values (60–210 kV cm^{-1}) are much higher than those in the ITPs.

Despite the similar P_s values for all x, the solid solutions [$A_xQ_{1-x}H$][ReO_4] are not isomorphous in the LTPs. The PXRD

patterns of $[A_xQ_{1-x}H][ReO_4]$ at 160 K (Figures 7 and S22), where all crystals were in their LTPs, illustrate that three different types of crystal structures are obtained depending on the composition: (1) For $0 \le x \le 0.6$, the patterns can be fitted to $Pmn2_1$ structures isomorphous with that of $[QH][ReO_4]$ ($x = 0$); the obtained lattice parameters are listed in Table S7. (2) For $x = 0.9$ and 1 ($[AH][ReO_4]$), the crystals possess isomorphous structures. While indexing of the complex PXRD patterns for $x = 0.9$ and 1 failed, they are clearly not isostructural with the $Pmn2_1$ structure for $0 \le x \le 0.6$. (3) For $x = 0.7$ and 0.8, the solid solutions manifest a crystal structure different from those of the two aforementioned end members. The PXRD patterns of the newly appeared phase can be fitted to the lattice of the monoclinic crystal system with the space group Pc (Figure S23 and Table S7). These results are summarized in the phase diagram of $[A_xQ_{1-x}H][ReO_4]$ (Figure 8a), which demonstrates the first example of MPBs in plastic/ferroelectric crystals: $[AH][ReO_4]$ and $[QH][ReO_4]$ have different crystal structures in the LTPs, and their solid solutions show two MPBs with a newly produced monoclinic phase between them.

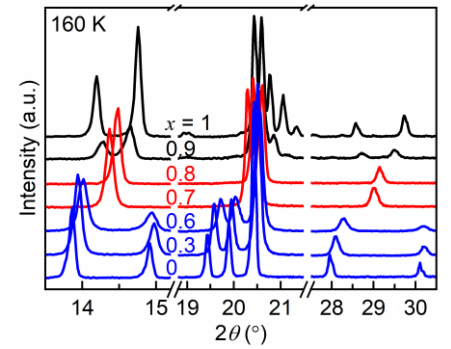

Figure 7. Powder X-ray diffraction patterns of $[A_xQ_{1-x}H][ReO_4]$ for selected x values at 160 K.

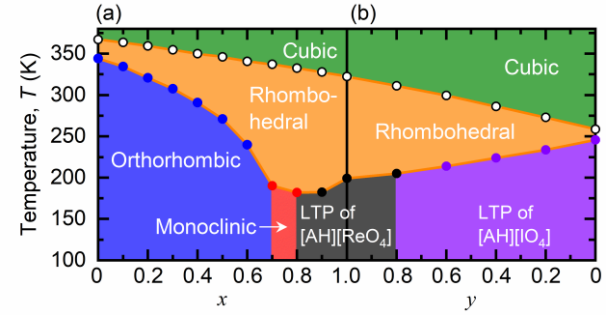

Figure 8. Composition–temperature phase diagrams of (a) $[A_xQ_{1-x}H][ReO_4]$ and (b) $[AH][Re_yI_{1-y}O_4]$.

The mixed-anion $[AH][Re_yI_{1-y}O_4]$ system also exhibits a morphotropic transition at low temperatures (Figure 8b). Similar to $[A_xQ_{1-x}H][ReO_4]$, all solid solutions $[AH][Re_yI_{1-y}O_4]$ are isostructural in the HTP (the cubic crystal) and ITP (the rhombohedral crystal) (Figure 2). Although the complex PXRD patterns in the LTP could not be indexed, the system exhibits a clear morphotropic transition between $y = 0.6$ and 0.8 (Figure S24). All $[AH][Re_yI_{1-y}O_4]$ crystals exhibited ferroelectricity in their LTPs as demonstrated by P–E hysteresis measurements (Figure S12). The P_s values in the LTPs in the range $y = 0$–0.6, in which the system is isostructural with $[AH][IO_4]$, are smaller than the corresponding ones in the ITP. In contrast, the P_s values in the LTPs for $y = 0.8$ and 1, where the system is isostructural with $[AH][ReO_4]$, are comparable or slightly larger than those in the ITP. Although the different behavior of the P_s values with variation of y is consistent with the presence of an MPB, the origins remain elusive at present due to a lack of detailed information regarding the crystal structures.

The MPBs found in the $[AH][Re_yI_{1-y}O_4]$ and $[A_xQ_{1-x}H][ReO_4]$ systems occur significantly below room temperature (~200 K or below), and the properties of these materials, including piezoelectricity, were not examined in the vicinity of the MPBs. However, the occurrence of MPBs in solid solutions of plastic/ferroelectric crystals can be expected to stimulate an extensive exploration and investigation of MPBs and related phenomena in this molecular ferroelectric crystal family. These efforts will eventually lead to an expansion of the rich materials science of MPBs, which has thus far focused on inorganic oxides.

CONCLUSIONS

In summary, we have succeeded in preparing all-proportional solid solutions and property tuning of plastic/ferroelectric crystals of 1-azabicyclo[2.2.1]heptanium perrhenate ($[AH][ReO_4]$). The obtained solid solutions maintain the ferroelectric performance of the parent ferroelectric crystals, *i.e.*, low-electric-field switching and high pyroelectricity, in the intermediate-temperature phase (ITP). The formation of solid solutions allowed a continuous tuning of the Curie temperature (T_C) of the ferroelectric system over a range of 100 K. Through this adjustment of the T_C, the pyroelectric performance of the system can be flexibly tuned and the $|p|$, $|F_v|$, and k^2 values significantly enhanced at room temperature. Moreover, the solid solutions exhibit morphotropic phase boundaries (MPBs) in the composition–temperature phase diagrams.

The results of this work also underscore the importance of a suitable procedure for producing solid solutions. By using a rapid-precipitation technique that has not yet been commonly employed, we were able to prepare solid solutions of molecular ferroelectric crystals that have not yet been obtained by means of conventional methods. Solid solutions of molecular crystals have typically been prepared by either solidification from the molten state or slow growth from solution. Single crystals obtained through the latter method are highly valuable, as they allow determining the crystal structure of the solid solution by means of X-ray diffraction analysis. However, this preparation procedure is, in principle, a purification process, and it is thus difficult to obtain homogeneous solid solutions from it. Relying solely on this method, may, therefore, restrict studies on solid solutions. Further development of preparation techniques could potentially enable the formation of solid solutions that have hitherto been considered inaccessible via conventional methods and would lead to new insights into solid-solution-formation phenomena.

Using this rapid-precipitation method, we have demonstrated performance tuning and the manifestation of MPBs via the formation of solid solutions, which are unprecedented for plastic/ferroelectric crystals. This preparation technique can also be potentially applied to other plastic/ferroelectric crystals. A considerable number of plastic/ferroelectric ionic crystals have been developed based on the combination of cations and anions with globular molecular structures. While each crystal exhibits a variety of crystal structures and ferroelectric-performance patterns in the ferroelectric phase, most of these have cubic CsCl-type structures in the paraelectric plastic crystal phase. The

presence of this common aristotype is analogous to the fact that the ferroelectric inorganic oxide family has a common cubic perovskite aristotype, which should be advantageous for the formation of solid solutions. Systematically investigating the solid solutions of plastic/ferroelectric ionic crystals can be expected to result in the development of tailor-made materials that exhibit improved performance and ease of use. The broadened scope of materials development may also result in the discovery of a wealth of novel phenomena, thereby advancing the study of this ferroelectric family into a rich field of functional molecular science.

ASSOCIATED CONTENT

Supporting Information. The Supporting Information is available free of charge on the ACS Publications website at DOI: 10.1012/jacs.xxxxxxx.

Experimental procedures for measurements; powder X-ray diffraction patterns; DSC traces; analyzed molar ratios; lattice parameters; dielectric constants; *P–E* hysteresis loops; phase structures; pyroelectric measurements, fitted parameters for estimation of pyroelectric coefficients and related indices; specific heat capacity, references (PDF)

AUTHOR INFORMATION

Corresponding Author

* E-mail: junharada@sci.hokudai.ac.jp

Notes

The authors declare no competing financial interest.

ACKNOWLEDGMENT

This work was supported by JSPS KAKENHI Grant Numbers JP19H00884 and JP23H01931. The authors would like to thank Ms. N. Takeda for ICP-MS analyses (Hokkaido University) and Ms. E. Nishiura (Nitto Analytical Techno-Center) for LC-MS analyses. The authors would also like to thank Dr. D. Hashizume and Dr. M. Hoshino for fruitful discussions pertaining to powder diffraction data.

REFERENCES

(1) Lines, M. E.; Glass, A. M., *Principles and Applications of Ferroelectrics and Related Materials*; Clarendon Press: Oxford, 1977.

(2) (a) Horiuchi, S.; Tokura, Y., Organic ferroelectrics. *Nat. Mater.* **2008**, *7*, 357-366. (b) Shi, P.-P.; Tang, Y.-Y.; Li, P.-F.; Liao, W.-Q.; Wang, Z.-X.; Ye, Q.; Xiong, R.-G., Symmetry breaking in molecular ferroelectrics. *Chem. Soc. Rev.* **2016**, *45*, 3811-3827. (c) Zhang, H.-Y.; Tang, Y.-Y.; Shi, P.-P.; Xiong, R.-G., Toward the Targeted Design of Molecular Ferroelectrics: Modifying Molecular Symmetries and Homochirality. *Acc. Chem. Res.* **2019**, *52*, 1928-1938. (d) Liu, H.-Y.; Zhang, H.-Y.; Chen, X.-G.; Xiong, R.-G., Molecular Design Principles for Ferroelectrics: Ferroelectrochemistry. *J. Am. Chem. Soc.* **2020**, *142*, 15205-15218. (e) Horiuchi, S.; Ishibashi, S., Hydrogen-Bonded Small-Molecular Crystals Yielding Strong Ferroelectric and Antiferroelectric Polarizations. *J. Phys. Soc. Jpn.* **2020**, *89*, 051009. (f) Zhang, H.-Y.; Chen, X.-G.; Tang, Y.-Y.; Liao, W.-Q.; Di, F.-F.; Mu, X.; Peng, H.; Xiong, R.-G., PFM (piezoresponse force microscopy)-aided design for molecular ferroelectrics. *Chem. Soc. Rev.* **2021**, *50*, 8248-8278. (g) Liu, H.; Ye, Y.; Zhang, X.; Yang, T.; Wen, W.; Jiang, S., Ferroelectricity in organic materials: from materials characteristics to de novo design. *J. Mater. Chem. C* **2022**, *10*, 13676-13689. (h) Han, X.-B.; Chai, C.-Y.; Liang, B.-D.; Fan, C.-C.; Zhang, W., Ferroic phase transition molecular crystals. *CrystEngComm* **2022**, *24*, 1507-1517. (i) Pan, Q.; Gu, Z.-X.; Zhou, R.-J.; Feng, Z.-J.; Xiong, Y.-A.; Sha, T.-T.; You, Y.-M.; Xiong, R.-G., The past 10 years of molecular ferroelectrics: structures, design, and properties. *Chem. Soc. Rev.* **2024**, *53*, 5781-5861.

(3) Harada, J.; Shimojo, T.; Oyamaguchi, H.; Hasegawa, H.; Takahashi, Y.; Satomi, K.; Suzuki, Y.; Kawamata, J.; Inabe, T., Directionally tunable and mechanically deformable ferroelectric crystals from rotating polar globular ionic molecules. *Nat. Chem.* **2016**, *8*, 946-952.

(4) Harada, J., Plastic/ferroelectric molecular crystals: Ferroelectric performance in bulk polycrystalline forms. *APL Mater.* **2021**, *9*, 020901.

(5) (a) Timmermans, J., Plastic crystals: A historical review. *J. Phys. Chem. Solids* **1961**, *18*, 1-8. (b) Sherwood, J. N., *The Plastically Crystalline State: Orientationally Disordered Crystals*; Wiley: Chichester; New York, 1979. (c) Das, S.; Mondal, A.; Reddy, C. M., Harnessing molecular rotations in plastic crystals: a holistic view for crystal engineering of adaptive soft materials. *Chem. Soc. Rev.* **2020**, *49*, 8878-8896.

(6) (a) Fyfe, C. A., *Solid State NMR for Chemists*; CFC Press: Guelph, 1983. (b) Brand, R.; Lunkenheimer, P.; Loidl, A., Relaxation dynamics in plastic crystals. *J. Chem. Phys.* **2002**, *116*, 10386-10401. (c) Sun, Z.; Chen, T.; Liu, X.; Hong, M.; Luo, J., Plastic Transition to Switch Nonlinear Optical Properties Showing the Record High Contrast in a Single-Component Molecular Crystal. *J. Am. Chem. Soc.* **2015**, *137*, 15660-15663. (d) Sun, Y.-Z.; Huang, B.; Xu, W.-J.; Zhou, D.-D.; Chen, S.-L.; Zhang, S.-Y.; Du, Z.-Y.; Xie, Y.-R.; He, C.-T.; Zhang, W.-X.; Chen, X.-M., Plastic Crystals with Polar Halochromate Anion: Thermosensitive Dielectrics Based upon Plastic Transition and Dipole Rotation. *Inorg. Chem.* **2016**, *55*, 11418-11425. (e) Matsuki, M.; Yamada, T.; Yasuda, N.; Dekura, S.; Kitagawa, H.; Kimizuka, N., Nonpolar-to-Polar Phase Transition of a Chiral Ionic Plastic Crystal and Switch of the Rotation Symmetry. *J. Am. Chem. Soc.* **2018**, *140*, 291-297. (f) Yoneya, M.; Harada, J., Molecular Dynamics Simulation Study of the Plastic/Ferroelectric Crystal Quinuclidinium Perrhenate. *J. Phys. Chem. C* **2020**, *124*, 2171-2177. (g) Sato, C.; Takeda, T.; Dekura, S.; Suzuki, Y.; Kawamata, J.; Akutagawa, T., Chiral Plastic Crystal of Solid-State Dual Rotators. *Cryst. Growth Des.* **2023**, *23*, 5889-5898.

(7) (a) MacFarlane, D. R.; Forsyth, M., Plastic Crystal Electrolyte Materials: New Perspectives on Solid State Ionics. *Adv. Mater.* **2001**, *13*, 957-966. (b) Pringle, J. M.; Howlett, P. C.; MacFarlane, D. R.; Forsyth, M., Organic ionic plastic crystals: recent advances. *J. Mater. Chem.* **2010**, *20*, 2056-2062. (c) Zhu, H.; MacFarlane, D. R.; Pringle, J. M.; Forsyth, M., Organic Ionic Plastic Crystals as Solid-State Electrolytes. *Trends Chem.* **2019**, *1*, 126-140.

(8) (a) Li, B.; Kawakita, Y.; Ohira-Kawamura, S.; Sugahara, T.; Wang, H.; Wang, J.; Chen, Y.; Kawaguchi, S. I.; Kawaguchi, S.; Ohara, K.; Li, K.; Yu, D.; Mole, R.; Hattori, T.; Kikuchi, T.; Yano, S.-i.; Zhang, Z.; Zhang, Z.; Ren, W.; Lin, S.; Sakata, O.; Nakajima, K.; Zhang, Z., Colossal barocaloric effects in plastic crystals. *Nature* **2019**, *567*, 506-510. (b) Lloveras, P.; Aznar, A.; Barrio, M.; Negrier, P.; Popescu, C.; Planes, A.; Mañosa, L.; Stern-Taulats, E.; Avramenko, A.; Mathur, N. D.; Moya, X.; Tamarit, J. L., Colossal barocaloric effects near room temperature in plastic crystals of neopentylglycol. *Nat. Commun.* **2019**, *10*, 1803. (c) Aznar, A.; Lloveras, P.; Barrio, M.; Negrier, P.; Planes, A.; Mañosa, L.; Mathur, N. D.; Moya, X.; Tamarit, J.-L., Reversible and irreversible colossal barocaloric effects in plastic crystals. *J. Mater. Chem. A* **2020**, *8*, 639-647. (d) Moya, X.; Mathur, N. D., Caloric materials for cooling and heating. *Science* **2020**, *370*, 797-803. (e) Aznar, A.; Negrier, P.; Planes, A.; Mañosa, L.; Stern-Taulats, E.; Moya, X.; Barrio, M.; Tamarit, J.-L.; Lloveras, P., Reversible colossal barocaloric effects near room temperature in 1-X-adamantane (X=Cl, Br) plastic crystals. *Appl. Mater. Today* **2021**, *23*, 101023. (f) Salvatori, A.; Aguilà, D.; Aromí, G.; Mañosa, L.; Planes, A.; Lloveras, P.; Pardo, L. C.; Appel, M.; Nataf, G. F.; Giovannelli, F.; Barrio, M.; Tamarit, J. L.; Romanini, M., Large barocaloric effects in two novel ferroelectric molecular plastic crystals. *J. Mater. Chem. A* **2023**, *11*, 12140-12150.

(9) Tang, Y.-Y.; Li, P.-F.; Liao, W.-Q.; Shi, P.-P.; You, Y.-M.; Xiong, R.-G., Multiaxial Molecular Ferroelectric Thin Films Bring Light to Practical Applications. *J. Am. Chem. Soc.* **2018**, *140*, 8051-8059.

(10) (a) Li, P.-F.; Tang, Y.-Y.; Wang, Z.-X.; Ye, H.-Y.; You, Y.-M.; Xiong, R.-G., Anomalously rotary polarization discovered in

homochiral organic ferroelectrics. *Nat. Commun.* **2016**, *7*, 13635. (b) Ye, H.-Y.; Ge, J.-Z.; Tang, Y.-Y.; Li, P.-F.; Zhang, Y.; You, Y.-M.; Xiong, R.-G., Molecular Ferroelectric with Most Equivalent Polarization Directions Induced by the Plastic Phase Transition. *J. Am. Chem. Soc.* **2016**, *138*, 13175-13178. (c) Pan, Q.; Liu, Z.-B.; Zhang, H.-Y.; Zhang, W.-Y.; Tang, Y.-Y.; You, Y.-M.; Li, P.-F.; Liao, W.-Q.; Shi, P.-P.; Ma, R.-W.; Wei, R.-Y.; Xiong, R.-G., A Molecular Polycrystalline Ferroelectric with Record-High Phase Transition Temperature. *Adv. Mater.* **2017**, *29*, 1700831. (d) Tang, Y.-Y.; Li, P.-F.; Zhang, W.-Y.; Ye, H.-Y.; You, Y.-M.; Xiong, R.-G., A Multiaxial Molecular Ferroelectric with Highest Curie Temperature and Fastest Polarization Switching. *J. Am. Chem. Soc.* **2017**, *139*, 13903-13908. (e) You, Y.-M.; Tang, Y.-Y.; Li, P.-F.; Zhang, H.-Y.; Zhang, W.-Y.; Zhang, Y.; Ye, H.-Y.; Nakamura, T.; Xiong, R.-G., Quinuclidinium salt ferroelectric thin-film with duodecuple-rotational polarization-directions. *Nat. Commun.* **2017**, *8*, 14934. (f) Li, D.; Zhao, X.-M.; Zhao, H.-X.; Dong, X.-W.; Long, L.-S.; Zheng, L.-S., Construction of Magnetoelectric Composites with a Large Room-Temperature Magnetoelectric Response through Molecular–Ionic Ferroelectrics. *Adv. Mater.* **2018**, *30*, 1803716. (g) Harada, J.; Yoneyama, N.; Yokokura, S.; Takahashi, Y.; Miura, A.; Kitamura, N.; Inabe, T., Ferroelectricity and Piezoelectricity in Free-Standing Polycrystalline Films of Plastic Crystals. *J. Am. Chem. Soc.* **2018**, *140*, 346-354. (h) Yang, C.-K.; Chen, W.-N.; Ding, Y.-T.; Wang, J.; Rao, Y.; Liao, W.-Q.; Xie, Y.; Zou, W.; Xiong, R.-G., Directional Intermolecular Interactions for Precise Molecular Design of a High-Tc Multiaxial Molecular Ferroelectric. *J. Am. Chem. Soc.* **2019**, *141*, 1781-1787. (i) Wei, Z.-H.; Jiang, Z.-T.; Zhang, X.-X.; Li, M.-L.; Tang, Y.-Y.; Chen, X.-G.; Cai, H.; Xiong, R.-G., Rational Design of Ceramic-Like Molecular Ferroelectric by Quasi-Spherical Theory. *J. Am. Chem. Soc.* **2020**, *142*, 1995-2000. (j) Xie, Y.; Ai, Y.; Zeng, Y.-L.; He, W.-H.; Huang, X.-Q.; Fu, D.-W.; Gao, J.-X.; Chen, X.-G.; Tang, Y.-Y., The Soft Molecular Polycrystalline Ferroelectric Realized by the Fluorination Effect. *J. Am. Chem. Soc.* **2020**, *142*, 12486-12492. (k) Zhang, Y.; Song, X.-J.; Zhang, Z.-X.; Fu, D.-W.; Xiong, R.-G., Piezoelectric Energy Harvesting Based on Multiaxial Ferroelectrics by Precise Molecular Design. *Matter* **2020**, *2*, 697-710. (l) Wang, B.; Hong, J.; Yang, Y.; Zhao, H.; Long, L.; Zheng, L., Achievement of a giant piezoelectric coefficient and piezoelectric voltage coefficient through plastic molecular-based ferroelectric materials. *Matter* **2022**, *5*, 1296-1304. (m) Harada, J.; Takehisa, M.; Kawamura, Y.; Takahashi, H.; Takahashi, Y., Plastic/Ferroelectric Crystals with Distorted Molecular Arrangement: Ferroelectricity in Bulk Polycrystalline Films through Lattice Reorientation. *Adv. Electron. Mater.* **2022**, *8*, 2101415. (n) Harada, J.; Takahashi, H.; Notsuka, R.; Takehisa, M.; Takahashi, Y.; Usui, T.; Taniguchi, H., Ferroelectric Ionic Molecular Crystals with Significant Plasticity and a Low Melting Point: High Performance in Hot-Pressed Polycrystalline Plates and Melt-Grown Crystalline Sheets. *Angew. Chem., Int. Ed.* **2023**, *62*, e202215286. (o) Ai, Y.; Li, P.-F.; Chen, X.-G.; Lv, H.-P.; Weng, Y.-R.; Shi, Y.; Zhou, F.; Xiong, R.-G.; Liao, W.-Q., The First Ring Enlargement Induced Large Piezoelectric Response in a Polycrystalline Molecular Ferroelectric. *Adv.Sci.* **2023**, *10*, 2302426.

(11) (a) Jaffe, B.; Cook Jr., W. R.; Jaffe, H., *Piezoelectric Ceramics*; Academic Press: London and New York, 1971. (b) Haertling, G. H., Ferroelectric Ceramics: History and Technology. *J. Am. Ceram. Soc.* **1999**, *82*, 797-818.

(12) (a) Sawaguchi, E., Ferroelectricity versus Antiferroelectricity in the Solid Solutions of $PbZrO_3$ and $PbTiO_3$. *J. Phys. Soc. Jpn.* **1953**, *8*, 615-629. (b) Jaffe, B.; Roth, R. S.; Marzullo, S., Piezoelectric Properties of Lead Zirconate-Lead Titanate Solid-Solution Ceramics. *J. Appl. Phys.* **1954**, *25*, 809-810. (c) Fu, H.; Cohen, R. E., Polarization rotation mechanism for ultrahigh electromechanical response in single-crystal piezoelectrics. *Nature* **2000**, *403*, 281-283. (d) Noheda, B.; Cox, D. E.; Shirane, G.; Gao, J.; Ye, Z.-G., Phase diagram of the ferroelectric relaxor $(1-x)PbMg_{1/3}Nb_{2/3}O_3-xPbTiO_3$. *Phys. Rev. B* **2002**, *66*, 054104.

(13) Liao, W.-Q.; Zhao, D.; Tang, Y.-Y.; Zhang, Y.; Li, P.-F.; Shi, P.-P.; Chen, X.-G.; You, Y.-M.; Xiong, R.-G., A molecular perovskite solid solution with piezoelectricity stronger than lead zirconate titanate. *Science* **2019**, *363*, 1206-1210.

(14) Fan, C.-C.; Liu, C.-D.; Liang, B.-D.; Wang, W.; Jin, M.-L.; Chai, C.-Y.; Jing, C.-Q.; Ju, T.-Y.; Han, X.-B.; Zhang, W., Tuning ferroelectric phase transition temperature by enantiomer fraction. *Nat. Commun.* **2024**, *15*, 1464.

(15) Harada, J.; Kawamura, Y.; Takahashi, Y.; Uemura, Y.; Hasegawa, T.; Taniguchi, H.; Maruyama, K., Plastic/Ferroelectric Crystals with Easily Switchable Polarization: Low-Voltage Operation, Unprecedentedly High Pyroelectric Performance, and Large Piezoelectric Effect in Polycrystalline Forms. *J. Am. Chem. Soc.* **2019**, *141*, 9349-9357.

(16) (a) Kitaigorodsky, A. I., *Mixed Crystals*; Springer-Verlag: Berlin, 1984. (b) Cuevas-Diarte, M. À.; Oonk, H. A., *Molecular Mixed Crystals*. Springer: 2021. (c) Tsunashima, R., Molecular solid solutions for advanced materials – homeomorphic or heteromorphic. *CrystEngComm* **2022**, *24*, 1309-1318.

(17) Schur, E.; Nauha, E.; Lusi, M.; Bernstein, J., Kitaigorodsky Revisited: Polymorphism and Mixed Crystals of Acridine/Phenazine. *Chem. – Eur. J.* **2015**, *21*, 1735-1742.

(18) (a) d'Agostino, S.; Fornasari, L.; Braga, D., Binary and Ternary Solid Solutions of Ionic Plastic Crystals, and Modulation of Plastic Phase Transitions. *Cryst. Growth Des.* **2019**, *19*, 6266-6273. (b) Lan, X.; Wang, X.; Zhang, D. X.; Mu, T.; Lan, X. Z., Cation and Anion Transfer in Quinuclidinium Hexafluorophosphate Plastic Crystal: Role of Constituent Ions and the Crystalline Structure. *J. Phys. Chem. C* **2021**, *125*, 21169-21178. (c) Ocak, S.; Birolo, R.; Carì, G.; Bordignon, S.; Chierotti, M. R.; Braga, D.; Gobetto, R.; Salzillo, T.; Venuti, E.; Yaffe, O.; d'Agostino, S., Engineering plastic phase transitions via solid solutions: the case of "reordering frustration" in ionic plastic crystals of hydroxyquinuclidinium salts. *Mol. Syst. Des. Eng.* **2022**, *7*, 950-962.

(19) Matsumoto, K.; Nonaka, R.; Wang, Y.; Veryasov, G.; Hagiwara, R., Formation of a solid solution between $[N(C_2H_5)_4][BF_4]$ and $[N(C_2H_5)_4][PF_6]$ in crystal and plastic crystal phases. *Phys. Chem. Chem. Phys.* **2017**, *19*, 2053-2059.

(20) MacFarlane, D. R.; Huang, J.; Forsyth, M., Lithium-doped plastic crystal electrolytes exhibiting fast ion conduction for secondary batteries. *Nature* **1999**, *402*, 792-794.

(21) (a) Scott, J. F., Electrocaloric Materials. *Annu. Rev. Mater. Res.* **2011**, *41*, 229-240. (b) Correia, T.; Zhang, Q., *Electrocaloric materials*. *New Generation of Coolers*; Springer: Berlin 2014. (c) Moya, X.; Kar-Narayan, S.; Mathur, N. D., Caloric materials near ferroic phase transitions. *Nat. Mater.* **2014**, *13*, 439-450. (d) Ji, H.-R.; Zhou, R.-J.; Yao, J.; Cao, X.-X.; Jing, Z.-Y.; Pan, Q.; Feng, Z.-J.; Gu, Z.-X.; You, Y.-M., Giant electrocaloric effect in a molecular ceramic. *Mater. Horiz.* **2023**, *10*, 869-874.

(22) (a) Vegard, L., Die Konstitution der Mischkristalle und die Raumfüllung der Atome. *Z. Phys.* **1921**, *5*, 17-26. (b) Vegard, L.; Dale, H., VIII. Untersuchungen über Mischkristalle und Legierungen. *Z. Krist.* **1928**, *67*, 148-162.

(23) (a) Whatmore, R. W., Pyroelectric devices and materials. *Rep. Prog. Phys.* **1986**, *49*, 1335-1386. (b) Lang, S. B.; Das-Gupta, D. K. Pyroelectricity: Fundamentals and applications. In *Handbook of Advanced Electronic and Photonic Materials and Devices*; Singh Nalwa, H., Ed.; Academic Press: Burlington, 2001; Chapter 1, pp 1-55. (c) Lang, S. B., Pyroelectricity: From Ancient Curiosity to Modern Imaging Tool. *Phys. Today* **2005**, *58*, 31-36. (d) Bowen, C. R.; Taylor, J.; LeBoulbar, E.; Zabek, D.; Chauhan, A.; Vaish, R., Pyroelectric materials and devices for energy harvesting applications. *Energy Environ. Sci.* **2014**, *7*, 3836-3856.

(24) In reference 15, the $|p|$ value of polycrystalline $[AH][ReO_4]$ was reported to be 0.015 $\mu C\ cm^{-2}\ K^{-1}$ (=150 $\mu C\ m^{-2}\ K^{-1}$) at 298 K based on the pyroelectric current data measured using a constant-temperature-ramp method. In this method, the temperature dependence of P_s is obtained by integrating the current as a function of time, and the $|p|$ values are evaluated by differentiating P_s with respect to the temperature. The obtained $|p|$ values as a function of temperature were reproduced well using the present values obtained from the temperature-oscillation method (Figure S15). Conversely, the previous $|p|$ data obtained through the differentiation displayed some variation. Among the fluctuating data, a somewhat smaller $|p|$ value at 298 K and correspondingly smaller $|F_v|$ and k^2 values were reported.

For Table of Contents Only